

The SpoVA membrane complex is required for dipicolinic acid import during sporulation and export during germination

Yongqiang Gao,¹ Rocio Del Carmen Barajas-Ornelas,¹ Jeremy D. Amon,¹
Fernando H. Ramírez-Guadiana,¹ Assaf Alon,² Kelly P. Brock,³ Debora S. Marks,^{3,4} Andrew C. Kruse,²
and David Z. Rudner¹

¹Department of Microbiology, Harvard Medical School, Boston, Massachusetts 02115, USA; ²Department of Biological Chemistry and Molecular Pharmacology, Harvard Medical School, Boston, Massachusetts 02115, USA; ³Department of Systems Biology, Harvard Medical School, Boston, Massachusetts 02115, USA; ⁴Broad Institute of Harvard and Massachusetts Institute of Technology, Cambridge, Massachusetts 02142, USA

In response to starvation, endospore-forming bacteria differentiate into stress-resistant spores that can remain dormant for years yet rapidly germinate and resume growth in response to nutrients. The small molecule dipicolinic acid (DPA) plays a central role in both the stress resistance of the dormant spore and its exit from dormancy during germination. The *spoVA* locus is required for DPA import during sporulation and has been implicated in its export during germination, but the molecular bases are unclear. Here, we define the minimal set of proteins encoded in the *Bacillus subtilis* *spoVA* operon required for DPA import and demonstrate that these proteins form a membrane complex. Structural modeling of these components combined with mutagenesis and *in vivo* analysis reveal that the C and Eb subunits form a membrane channel, while the D subunit functions as a cytoplasmic plug. We show that point mutations that impair the interactions between D and the C–Eb membrane complex reduce the efficiency of DPA import during sporulation and reciprocally accelerate DPA release during germination. Our data support a model in which DPA transport into spores involves cycles of unplugging and then replugging the C–Eb membrane channel, while nutrient detection during germination triggers DPA release by unplugging it.

[Keywords: sporulation; germination; dormancy; dipicolinic acid; DPA; spoVA]

Supplemental material is available for this article.

Received February 14, 2022; revised version accepted May 16, 2022.

The singular goal of the developmental process of sporulation is to produce a dormant, stress-resistant spore that can rapidly germinate and resume growth in response to nutrients (Moir and Cooper 2015; Setlow et al. 2017; Shen et al. 2019). Central to this goal is the small molecule pyridine-2,6-dicarboxylic acid (dipicolinic acid [DPA]) (Setlow 2014). All spores derived from pathogenic and nonpathogenic endospore-forming bacteria contain very high concentrations of DPA in their core, accounting for 5%–14% of the spore dry weight. DPA is thought to protect the spore chromosome and displace water, resulting in core dehydration and providing resistance to UV radiation, heat, and desiccation. One of the earliest steps in the exit from dormancy is the expulsion of DPA from the core (Moir and Cooper 2015; Setlow et al. 2017; Shen et al. 2019), which activates cell wall lytic enzymes that degrade the specialized peptidoglycan cortex that surrounds the spore. DPA and its contribution to spore resistance were discovered almost 70 yr ago (Powell 1953), but

the molecular bases for its import into spores during sporulation and its export during germination remain poorly understood.

DPA is produced at a late stage in sporulation in the mother cell that nurtures the developing endospore inside it. Two proteins (SpoVFA and SpoVFB) expressed in the mother cell at this stage convert dihydroxydipicolinic acid, an intermediate in the lysine biosynthetic pathway, into DPA (Bach and Gilvarg 1966; Daniel and Errington 1993). DPA is then translocated across the two membranes that separate the mother cell and prospective spore (Fig. 1A), where it accumulates as a Ca^{2+} chelate (Setlow 2014). Our previous studies identified SpoVV as the mother cell membrane protein that transports DPA across the outer spore membrane (Ramírez-Guadiana et al. 2017a). Work over the last two decades has provided strong evidence that the proteins encoded in the *spoVA* (5A) operon

© 2022 Gao et al. This article is distributed exclusively by Cold Spring Harbor Laboratory Press for the first six months after the full-issue publication date [see <http://genesdev.cshlp.org/site/misc/terms.xhtml>]. After six months, it is available under a Creative Commons License [Attribution-NonCommercial 4.0 International], as described at <http://creativecommons.org/licenses/by-nc/4.0/>.

Corresponding author: rudner@hms.harvard.edu

Article published online ahead of print. Article and publication date are online at <http://www.genesdev.org/cgi/doi/10.1101/gad.349488.122>.

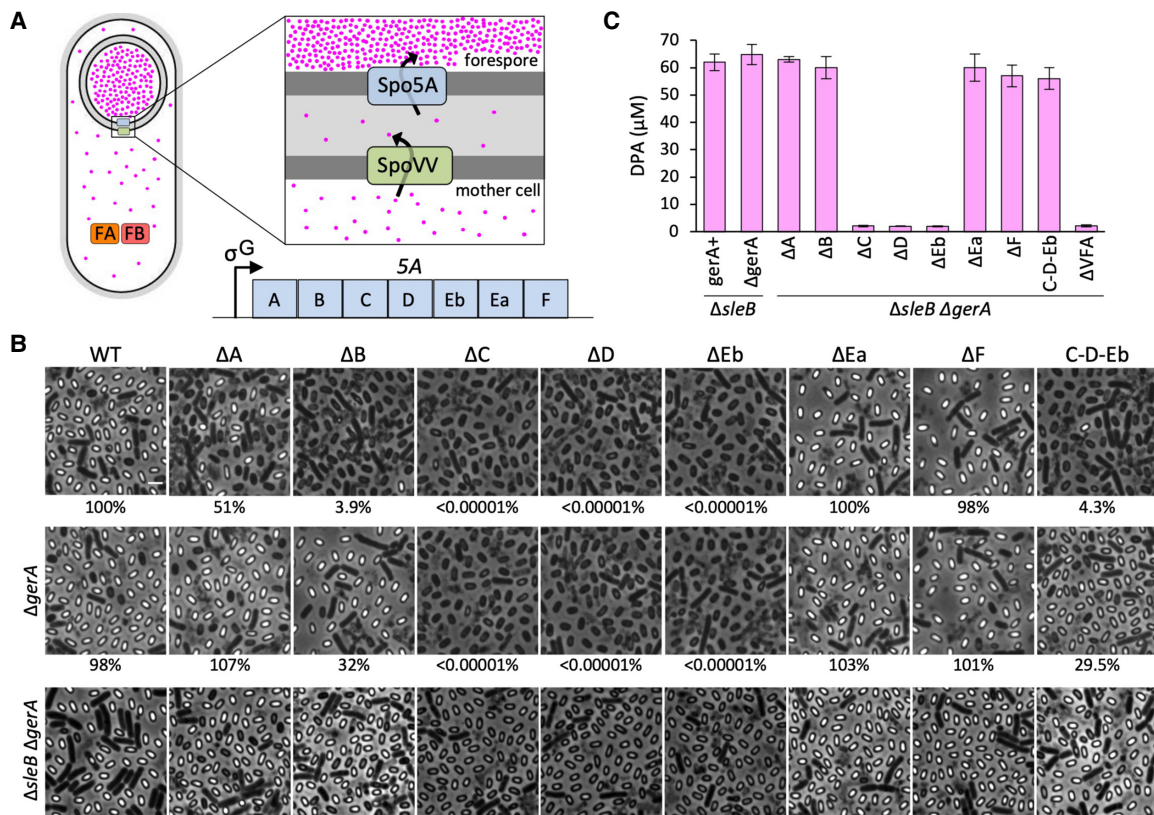


Figure 1. A minimal set of 5A proteins required for DPA accumulation. (A) Schematic model of DPA import into the prospective spore during sporulation. DPA (pink circle) is synthesized in the mother cell by SpoVFA (FA) and SpoVFB (FB) and transported across the outer forespore membrane by SpoVV. It is then likely transported across the inner forespore membrane by proteins encoded in the *spoVA* (5A) operon that are synthesized in the forespore under the control of σ^G . (B) Representative phase-contrast images of sporulated cultures of the indicated mutants in the presence and absence of *gerA* and *sleB*. A $\Delta 5A$ mutant that expresses *C*, *D*, and *Eb* (C-D-Eb) from an ectopic locus is also shown. Sporulation efficiencies based on heat resistance (20 min at 80°C) are provided below the first two sets of images. Spores that lack DPA and SleB are unable to germinate, so sporulation efficiencies are not provided for the mutants in the $\Delta sleB$ background. Scale bar, 2 μ m. (C) Bar graph showing DPA levels in spores from the indicated strains. Total spores were isolated using lysozyme followed by SDS, normalized, and then boiled to release DPA. DPA in the supernatant was mixed with $TbCl_3$ and detected by fluorimetry.

are required for DPA accumulation in the spore core and likely transport it across the inner spore membrane (Tovar-Rojo et al. 2002; Li et al. 2012; Berendsen et al. 2016a,b; Donnelly et al. 2016; Francis and Sorg 2016; Baloh and Sorg 2021). The 5A operon in *B. subtilis* encodes seven proteins (A, B, C, D, Eb, Ea, and F) (Fig. 1A) that are expressed in the prospective spore at a late stage in spore development (Fort and Errington 1985; Wang et al. 2006). These proteins are broadly conserved among endospore formers (Paredes-Sabja et al. 2011; Berendsen et al. 2016a). Many of these bacteria contain the entire seven-gene operon; others lack one or more genes. However, in all cases, *C*, *D*, and *Eb* are present. *Clostridioides difficile*, for example, possesses only these three genes (Donnelly et al. 2016; Francis and Sorg 2016; Baloh and Sorg 2021).

Most of the 5A proteins lack sequence homology with proteins of known function. *C* and *Eb* are paralogs and *D* has structural homology with thiolase fold-containing enzymes including β -ketoacyl and polyketide synthases (Li et al. 2012), the significance of which is unclear. Using the crystal structure of the *D* protein, DPA could be com-

putationally docked into a conserved solvent-exposed pocket, and ligand-binding studies found a low-affinity interaction between *D* and DPA. Based on an earlier study that suggested *D* is located outside the spore cytoplasm (Korza and Setlow 2013), it was proposed that *D* functions like a substrate-binding protein of an ABC transporter, delivering DPA to a putative transport complex (Li et al. 2012). Whether these proteins form a complex and, if so, how they function in DPA import remain unresolved.

The role of the 5A proteins in DPA export during germination is even less clear. Because mutations in the 5A genes prevent accumulation of DPA in spores, analysis of the effect of these mutations on DPA release has been impossible. An early study identified a temperature-sensitive 5A mutant and demonstrated that spores produced at the permissive temperature were impaired in DPA release when germinated at the restrictive temperature (Vepachedu and Setlow 2004). However, the mutation was found to be a single base change in the ribosome-binding site of the *C* gene, making it difficult to interpret the temperature sensitivity of the *C* protein. In the only

biochemical study on DPA transport, the C protein was reconstituted into proteoliposomes and was shown to have mechanosensitive channel-like properties (Velásquez et al. 2014), suggesting that changes in membrane tension upon nutrient detection could trigger DPA release. Whether and how the 5A proteins are involved in DPA release during germination have remained outstanding questions for decades.

Here, we demonstrate that C, D, and Eb are necessary and sufficient for DPA accumulation in dormant spores and show that these three proteins assemble into a membrane complex. Structural modeling of these components combined with mutational analysis suggests that C and Eb form a membrane channel and D functions as a cytoplasmic plug. We demonstrate that mutations that impair the interaction between C and D not only reduce the efficiency of DPA import during sporulation but also initiate DPA release faster than wild type during germination. Finally, we identify residues in a flexible loop of D that interact with the cytosolic entrance to the putative channel and have the properties of a plug. Our data support a model in which transport of DPA into the developing spore involves continuous rounds of unplugging and replugging of the channel, allowing the transporter to achieve an alternating access mechanism of membrane translocation. During germination, the removal of D in response to nutrient detection opens the channel, allowing DPA to flow down its concentration gradient.

Results

A minimal set of 5A proteins required for DPA accumulation in the developing spore

To investigate which 5A proteins in *B. subtilis* are required for DPA accumulation in the developing spore, we generated in-frame deletions of each of the seven genes in the 5A operon and analyzed their mutant phenotypes. As reported previously, the ΔA mutant was modestly impaired in sporulation efficiency (51%) and produced a mixture of phase-bright and prematurely germinated phase-dark or lysed spores (Fig. 1B; Ramírez-Guadiana et al. 2017b). Similarly, the ΔB mutant was reduced to 4% sporulation efficiency, and most spores appeared phase-dark. In contrast, sporulating cells lacking C, D, or Eb produced no viable spores, and phase-bright spores were undetectable (Fig. 1B; Tovar-Rojo et al. 2002; Li et al. 2012). Finally, cells lacking Ea or F sporulated at wild-type levels and produced abundant phase-bright spores (Fig. 1B; Perez-Valdespino et al. 2014). Previous studies suggest that premature germination and the production of phase-dark spores during sporulation can be due to impaired accumulation of DPA that leads to inappropriate activation of the GerA germinant receptor (Ramírez-Guadiana et al. 2017b). We therefore investigated whether the reduction in sporulation efficiency and phase-bright spores in the deletion mutants could be suppressed in the absence of GerA. As can be seen in Figure 1B and [Supplemental Figure S1](#), $\Delta gerA$ largely suppressed the ΔA and ΔB mutant phenotypes but had no impact on sporulating cells lacking C, D, or Eb.

To determine whether the mutant spores contained DPA, we purified total spores from the in-frame mutants in a $\Delta gerA \Delta sleB$ background. The $\Delta gerA$ mutation was included to suppress premature germination in the ΔA and ΔB mutants, and $\Delta sleB$ was included because its product (SleB) is responsible for degradation of the cortex peptidoglycan during premature germination (Moriyama et al. 1996; Heffron et al. 2011; Amon et al. 2021). Accordingly, the $\Delta sleB$ mutant ensured retention of this protective layer in the ΔC , ΔD , and ΔEb mutants. As can be seen in Figure 1B, the inclusion of $\Delta sleB$ resulted in intact phase-gray spores in these mutants. Spore cultures were treated with lysozyme followed by SDS to remove vegetative cells and cortexless phase-dark spores. Equivalent amounts of purified spores were boiled to release DPA, and the levels in the supernatant were monitored using $TbCl_3$. Figure 1C shows that purified spores derived from mutants lacking A, B, Ea, or F accumulated wild-type levels of DPA. In contrast and consistent with their phase-gray appearance, ΔC , ΔD , and ΔEb spores lacked DPA, with $TbCl_3$ -DPA fluorescence levels similar to a $\Delta spoVFA$ (ΔVFA) mutant lacking the DPA synthase (Fig. 1C; [Supplemental Fig. S1](#)). Similar findings have been reported for the C, D, and Eb orthologs in *C. difficile* (Donnelly et al. 2016; Francis and Sorg 2016; Baloh and Sorg 2021). Importantly, all 5A mutants could be complemented for sporulation efficiency and DPA accumulation by expression of the deleted gene in *trans* ([Supplemental Fig. S2](#)), indicating that the mutant phenotypes were not due to polar effects.

These data indicate that C, D, and Eb are required for DPA accumulation in the developing spores. To determine whether these three proteins are sufficient, we generated a strain lacking the entire 5A operon and expressed C, D, and Eb from an ectopic locus. The mutant had 4% sporulation efficiency in a $gerA^+$ background and 29.5% efficiency in the $\Delta gerA$ mutant (Fig. 1B; [Supplemental Fig. S3](#)). Importantly, the purified spores accumulated DPA to levels similar to wild type (Fig. 1C; [Supplemental Fig. S1](#)). These data are consistent with the idea that C, D, and Eb represent the minimal set of 5A proteins required for DPA transport into the developing spore.

C, D, and Eb form a membrane complex

As a first step toward characterizing the 5A proteins in vivo, we generated functional His-tagged fusions to A, C, D, Eb, Ea, and F expressed under the native 5A promoter ([Supplemental Fig. S4A,B](#)). We then monitored the stability of each fusion in purified spores in the presence and absence of the 5A locus. For these experiments, the strains contained the $\Delta sleB$ mutant to prevent degradation of the cortex peptidoglycan, enabling spore purification for immunoblot analysis. As can be seen in Figure 2A, the levels of D-His, Ea-His, and F-His were similar in the presence or absence of the other 5A proteins. In contrast, the levels of His-C and Eb-His were undetectable in the $\Delta 5A$ mutant, and the level of A-His was reduced (Fig. 2A). To determine which 5A proteins were required for the stability of A, C, and Eb, we analyzed protein levels of each in spores derived from the in-frame deletion

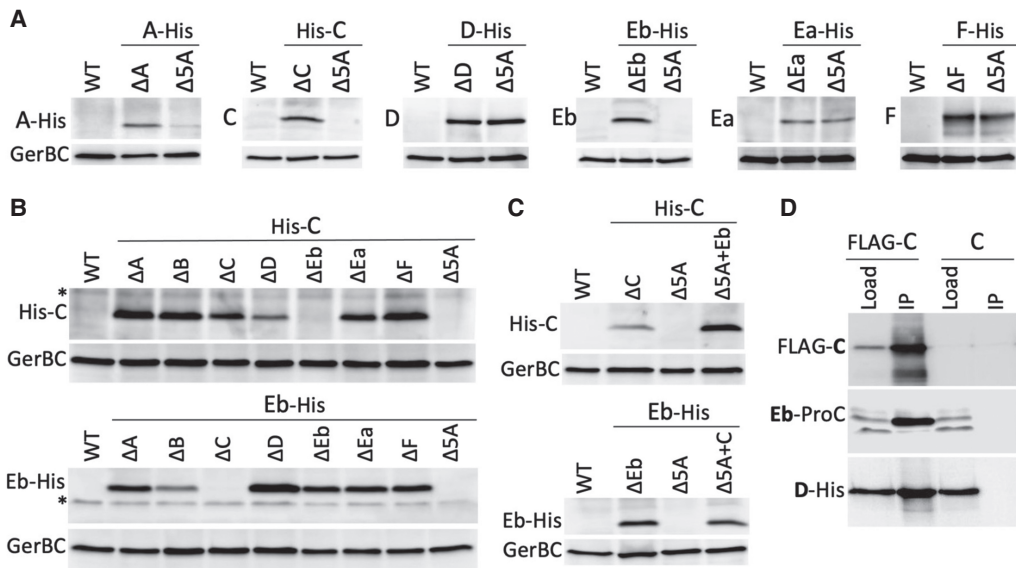


Figure 2. C, D, and Eb assemble into a membrane complex. (A) His-tagged fusions to A, C, and Eb are unstable in spores lacking the 5A locus. Representative anti-His immunoblots from spore lysates of the indicated strains. GerBC controlled for loading. (B) Stability of His-C and Eb-His in spores from strains lacking individual 5A genes. Cross-reacting bands are indicated with asterisks. (C) C and Eb stabilize each other in the absence of all other 5A proteins. All strains used in A–C were $\Delta sleB$ to prevent cortex degradation, enabling spore purification for immunoblot analysis. (D) Representative immunoblots showing copurification of FLAG-C, Eb-ProC, and D-His using anti-FLAG resin. The *B. cereus* 5A-1 proteins were coexpressed in *E. coli*, and detergent-solubilized membrane preparations (Load) were subjected to immunopurification (IP) on anti-FLAG resin.

mutants. As above, all strains contained the $\Delta sleB$ mutation. His-C was undetectable in spores lacking Eb and, reciprocally, Eb-His was undetectable in spores lacking C (Fig. 2B). In addition, the levels of His-C were partially reduced in the absence of D, and the levels of Eb-His were reduced in the absence of B. Finally, the reduced level of A-His in spores lacking the 5A locus was similar to spores lacking B (Supplemental Fig. S4C). Collectively, these data indicate that C and Eb depend on each other for stability and could therefore form a complex. Furthermore, these data suggest that D, B, and A are present in the C-Eb complex or form subcomplexes with C and/or Eb. Consistent with the model that C and Eb form a complex, we found that coexpression of His-C and Eb or C and Eb-His in a strain lacking all the other genes in the 5A locus was sufficient to stabilize the His-tagged proteins (Fig. 2C).

The C and Eb paralogs are predicted to contain four transmembrane helices each. To investigate whether they form a membrane complex, we coexpressed epitope-tagged versions in *E. coli*. However, the proteins were produced at very low levels and appeared to aggregate. Coexpression of B and D did not ameliorate these problems. Instead, we turned to the homologous SpoVA-1 proteins from *Bacillus cereus*. The SpoVAC-1, SpoVAD-1, and SpoVAEB-1 subunits are 72%, 68%, and 73% identical to their *B. subtilis* orthologs. We coexpressed a FLAG-tagged variant of SpoVAC-1 (FLAG-C), a protein C fusion to SpoVEB-1 (Eb-ProC), and a His-tagged variant of SpoVAD-1 (D-His) in *E. coli*. A membrane fraction was isolated, and the proteins were solubilized with a

nonionic detergent. The detergent-solubilized proteins were subjected to immuno-affinity purification using anti-FLAG resin, and the eluate was resolved by SDS-PAGE followed by Coomassie staining and immunoblot analysis. Figure 2D shows that Eb-ProC and D-His copurified with the C subunit, provided it was FLAG-tagged. The Coomassie-stained gel contained proteins of the expected sizes in the FLAG-C purification (Supplemental Fig. S5) that were confirmed to be FLAG-C, Eb-ProC, and D-His by mass spectrometry. Collectively, these data argue that C, Eb, and D, the minimal set of 5A proteins required for DPA accumulation, form a membrane complex.

D contacts the C-Eb membrane complex on the cytoplasmic face of the membrane

We used AlphaFold2 (Jumper et al. 2021; Mirdita et al. 2021) to investigate the C-D-Eb complex. The algorithm predicted a high-confidence C-Eb heterodimer with D docked on one face of the membrane complex with extensive contacts between D and the N terminus of C (Fig. 3A). The interresidue distance errors in the model were very low ($pTM > 0.91$), and the model's confidence in the positions of individual residues was very high ($pLDDT > 95$) (Supplemental Fig. S6A,B). Membrane topology prediction programs (Sonnhammer et al. 1998; Krogh et al. 2001; Kall et al. 2007) place the N terminus of C in the cytoplasm, suggesting that D interacts with the cytoplasmic face of the C-Eb complex (Fig. 3A). However, previous protease and amine-reactive biotin accessibility studies placed the D subunit outside the spore core in the

integument layers despite the absence of a signal sequence (Korza and Setlow 2013). To investigate this discrepancy, we constructed a functional GFP fusion to D (Supplemental Fig. S7A) and analyzed its localization in dormant spores. Functional GFP fusions to C and Eb (Supplemental Fig. S7A) were also generated as controls and, as anticipated, both localized in the spore membrane (Fig. 3B). A similar localization pattern was observed for D-GFP. Moreover, and consistent with the AlphaFold prediction, D-GFP localized in the cytoplasm in spores lacking the 5A locus (Fig. 3B; Supplemental Fig. S7B). Importantly, D-GFP remained full length in the $\Delta 5A$ mutant (Fig. 3C), indicating that the D-GFP fusion, and not a cleaved GFP, was responsible for the cytoplasmic localization.

To determine which 5A proteins are required for the membrane localization of D-GFP, we analyzed in-frame deletions of the individual genes in the operon. As can be seen in Figure 3D, ΔA , ΔEa , and ΔF mutant spores retained membrane-localized D-GFP, while ΔB , ΔC , and ΔEb spores had cytoplasmic D-GFP. Importantly, D-GFP was also membrane-localized in ΔVFA mutant spores that lack DPA (Fig. 3D). Thus, the cytoplasmic D-GFP localization in spores lacking B, C, or Eb was not due to the absence of DPA. Altogether, these cytological data are consistent with the AlphaFold prediction (Fig. 3A) and our in vitro studies (Fig. 2D) and argue that D interacts with the cytoplasmic face of the membrane complex composed of C and Eb. Our cytological analysis also suggests that the B protein helps localize D at the membrane; however, its role in the C-Eb complex remains unclear.

Intermolecular contacts between C and D

To validate the predicted interaction between D and the N terminus of C (Fig. 4A), we performed an evolutionary co-variation analysis (Marks et al. 2011; Hopf et al. 2012). This approach relies on the fact that amino acids involved in intermolecular interactions tend to coevolve with one another to maintain their interactions. Thus, evolutionarily coupled (EC) residue pairs generally reside in close proximity. We identified eight EC residue pairs in D and the N terminus of C with probability scores ≥ 0.9 (Fig. 4A; Supplemental Fig. S8; Hopf et al. 2012). All eight are consistent with the AlphaFold model. To validate these predictions, we generated a series of amino acid substitutions in four EC residues (N7, K11, Y15, and Q16) in the N terminus of C (Fig. 4A). Sporulation efficiency was modestly impaired in the single mutants but further decreased in the double, triple, and quadruple mutants (Fig. 4B). The decrease correlated with an increase in prematurely germinated phase-dark spores (Supplemental Fig. S9). Importantly, the premature germination and sporulation defects could be suppressed in a $\Delta gerA$ background (Supplemental Fig. S9), supporting the idea that these mutants are impaired in DPA accumulation. Furthermore, the stability of Eb-His was unaffected in the quadruple C [C(quad)] mutant (Fig. 4E), suggesting that the mutant subunit maintained its interaction with Eb and was therefore properly folded.

Next, we analyzed the localization of D-GFP in the C(quad) mutant spores. As above, the $\Delta sleB$ background was used to prevent cortex degradation in the prematurely

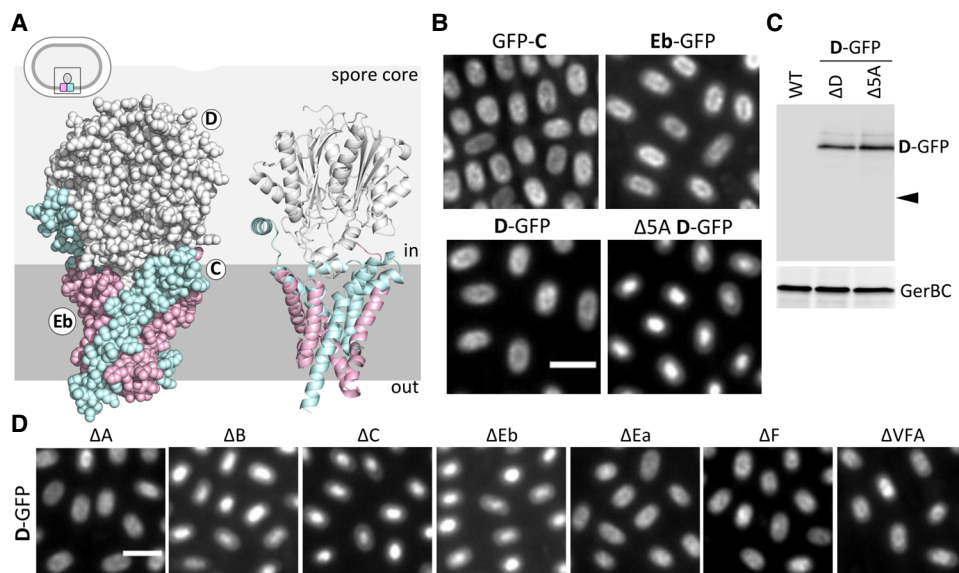


Figure 3. D interacts with the cytoplasmic face of the C-Eb membrane complex. **(A)** AlphaFold2-predicted structure of the C-D-Eb complex. C (cyan) and Eb (pink) form a membrane complex with interleaved transmembrane segments. The N terminus of C is predicted to be in the cytoplasm, where it interacts with D. **(B)** Representative fluorescent images of functional GFP fusions to C, Eb, and D in spores. In the absence of the 5A locus, D-GFP localizes in the spore cytoplasm. **(C)** D-GFP remains full length in the presence and absence of the 5A locus. Anti-GFP immunoblot from spore lysates of the indicated strains. The size of free GFP is indicated (arrowhead). GerBC controlled for loading. **(D)** Representative fluorescent images of D-GFP localization in spores of the indicated strains. All strains in *B-D* harbor $\Delta sleB$ to maintain the protective cortex layer. Scale bars, 2 μ m.

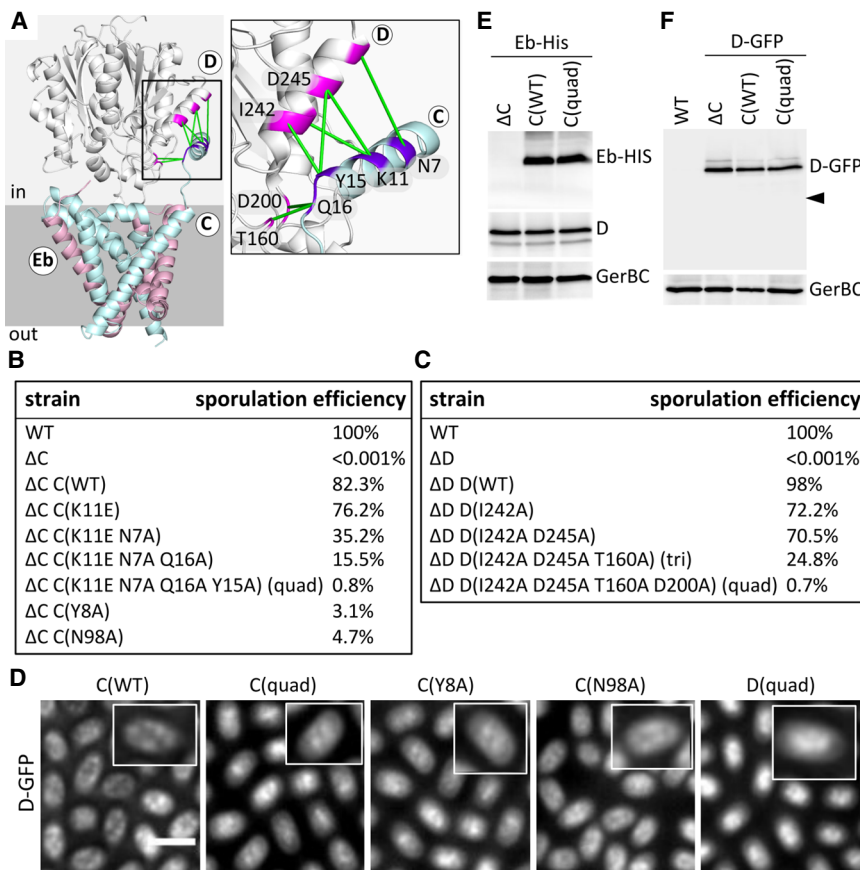


Figure 4. Intermolecular contacts between C and D. (A) AlphaFold model of C–D–Eb with highlighted evolutionarily coupled (EC) residue pairs. The EC pairs that were analyzed are labeled in the inset. (B,C) Sporulation efficiencies of the indicated C mutants (B) and D mutants (C). (D) Representative fluorescent images of D-GFP localization in purified phase-bright spores of the indicated strains. Insets show enlargements of individual spores with representative D-GFP localization. Scale bar, 2 μ m. (E) Eb-His is stable in C(quad) mutant spores. (F) D-GFP remains full length in C(quad) mutant spores. Anti-His and anti-GFP immunoblots from spore lysates of the indicated strains. D and GerBC controlled for loading. The size of free GFP is indicated (arrowhead). All strains in D–F harbor *AsleB* to maintain the protective cortex layer.

germinated spores. Most C(quad) spores phenocopied the ΔC mutant, appearing phase-gray, with D-GFP localized in the spore cytoplasm (Supplemental Fig. S10). However, ~1% of the spores were phase-bright with D-GFP displaying a patchy localization pattern (Supplemental Fig. S10). To confirm this phenotype, we purified the phase-bright spores in the C(quad) mutant using a Histodenz step gradient. Virtually all the purified phase-bright spores had patchy D-GFP localization (Fig. 4D) and, as expected, D-GFP remained full length (Fig. 4F). Similar results were obtained when we analyzed amino acid substitutions in EC residues (T160, D200, I242, and D245) in D (Fig. 4A,C,D; Supplemental Figs. S9, S10). We interpret this patchy localization pattern to be an intermediate phenotype in which some D-GFP localizes to the membrane-embedded C–Eb complex and some localizes to the spore cytoplasm.

In addition to substitutions in EC residue pairs, we analyzed a set of amino acid substitutions in highly conserved residues in C. One mutant, C(Y8A), phenocopied the C(quad) mutant with reduced sporulation efficiency, a high frequency of premature germination, and a patchy D-GFP membrane localization (Fig. 4B,D; Supplemental Figs. S9–S11). This conserved N-terminal tyrosine is predicted to contact D in the AlphaFold model. In contrast, three other amino acid substitutions in C (N98A, Q40A, and C36A) also had reduced sporulation efficiency and premature germination but displayed membrane-localized D-GFP that resembled wild type (Fig. 4B,D; Supple-

mental Figs. S9, S11). These conserved residues are part of transmembrane segments in C and are not predicted to interact with D. Since these mutants have defects in DPA accumulation similar to the C(quad) and C(Y8A) mutants but retained normal D-GFP localization, we conclude that the patchy D-GFP localization in the C(quad) and C(Y8A) mutants is likely due to a partial disruption of the interaction between C and D and not simply a result of defects in DPA import.

Collectively, these data validate the interaction between C and D in the C–D–Eb structural model (Fig. 4A) and suggest that mutations that reduce the ability of D to dock on the C–Eb complex are impaired in DPA import, resulting in premature germination of most spores. However, a small percentage of spores successfully accumulate DPA and bypass premature germination, becoming phase-bright and heat-resistant.

C and D mutant spores trigger DPA release faster than wild type in response to nutrients

Despite sporulation efficiencies as low as 1%, we were able to purify sufficient quantities of phase-bright spores from the C and D mutants described above to analyze DPA levels and germination efficiency. Although DPA accumulation was impaired in these mutants and frequently caused premature germination, the phase-bright spores that were produced had levels of DPA similar to wild

type (Fig. 5A). Using these purified spores, we investigated germination by monitoring DPA release upon nutrient addition. Separately, we monitored the reduction in optical density as the phase-bright spores transitioned to phase-dark, a consequence of activation of the cortex lytic enzymes. Strikingly, all the mutants that impaired the interaction between C and D and that displayed a patchy D-GFP localization initiated germination faster than wild type (Fig. 5B–D). This effect was reproducible regardless of germinant used (L-alanine or a mixture of asparagine, glucose, fructose, and K⁺ [AGFK]) and the method used for monitoring germination (Supplemental Figs. S12, S13). Importantly, the mutant spores had heat resistance properties similar to wild type, arguing that the more rapid initiation of germination was not due to incomplete core dehydration (Supplemental Fig. S14; Popham et al. 1995). Finally, purified C mutant spores that were not predicted to disrupt the interaction between C and D and had D-GFP localization similar to wild type initiated DPA release and a drop in optical density similar to wild type (Fig. 5B; Supplemental Figs. S11, S13).

Prompted by these findings, we investigated the phase-bright spores from the ΔB mutant. D-GFP had a patchy localization pattern in purified phase-bright ΔB spores. Furthermore, DPA levels were similar to wild type. Consistent with our findings with the C and D mutants, nutrient-triggered germination, assayed by DPA release and reduction in optical density, initiated faster than wild type (Fig. 5A,C; Supplemental Figs. S10, S12, S13). Collectively, these data provide the strongest evidence to date that the 5A proteins are involved in DPA export during germination and suggest that nutrient sensing triggers a loss of interaction between D and the C-Eb complex, leading to the release of DPA.

The patchy D-GFP membrane localization in the mutant spores and its correlation with faster DPA release dur-

ing germination prompted us to investigate whether the mutant spores retained their DPA over time. To do so, we incubated suspensions of purified spores at 37°C and monitored DPA in the buffer over a 4-d time course. Over the first 2 d, ~5% of the DPA in wild-type spores accumulated in the buffer (Supplemental Fig. S16A). During this same time period, we detected ~2.5-fold more DPA in the buffer of the mutant spores. However, after day 2, the DPA levels in the buffer of all the spore preparations remained stable (Supplemental Fig. S16A). Importantly, the percentages of heat-resistant spores were similar among the strains tested over the same time course (Supplemental Fig. S16B). Thus, if an interaction between D and the C-Eb complex is required to prevent leakage of DPA from the spore core, the D protein is largely positioned properly in the mutants despite its patchy localization. However, the modest increase in DPA accumulation in the buffer is consistent with a weaker interaction between D and the C-Eb complex and the faster release of DPA observed upon nutrient sensing.

D has plug-like properties

The structural model of the C-Eb complex contains a narrow channel that spans the lipid bilayer (Fig. 6A), with many of the conserved residues in the two subunits lining the lumen (Supplemental Fig. S6C). Interestingly, two amino acids (E152 and Y153) in a flexible loop of D appear to plug the opening on the cytoplasmic side (Fig. 6A,B). To investigate whether these residues have plug-like properties, we generated D variants with alanine substitutions at E152 and Y153. Single mutants had modest reductions in sporulation efficiency that correlated with an increase in phase-dark spores, while the double mutant had a synergistic reduction in sporulation efficiency and premature germination (Fig. 6C). Importantly, the D-GFP variants

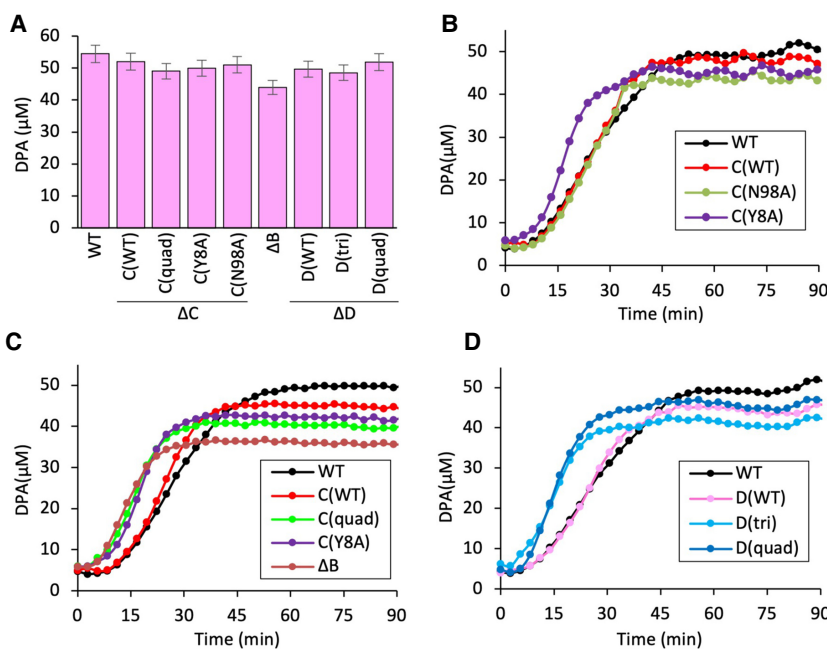


Figure 5. Spores with impaired interaction between C and D initiate germination faster in response to L-alanine. (A) Bar graph showing DPA levels in Histodenz-purified phase-bright spores of the indicated strains. (B–D) Spore germination in response to 1 mM L-alanine as assayed by release of DPA in the indicated strains. Purified phase-bright spores were induced to germinate with 1 mM L-alanine at time 0, and DPA release was monitored over time using TbCl₃. Supplemental Figure S12 shows phase-contrast images of the purified phase-bright spores, a biological replicate of the DPA release assay, and representative germination assays monitoring the drop in optical density. Supplemental Figure S15 shows that the phase-bright spores used in these assays were properly normalized.

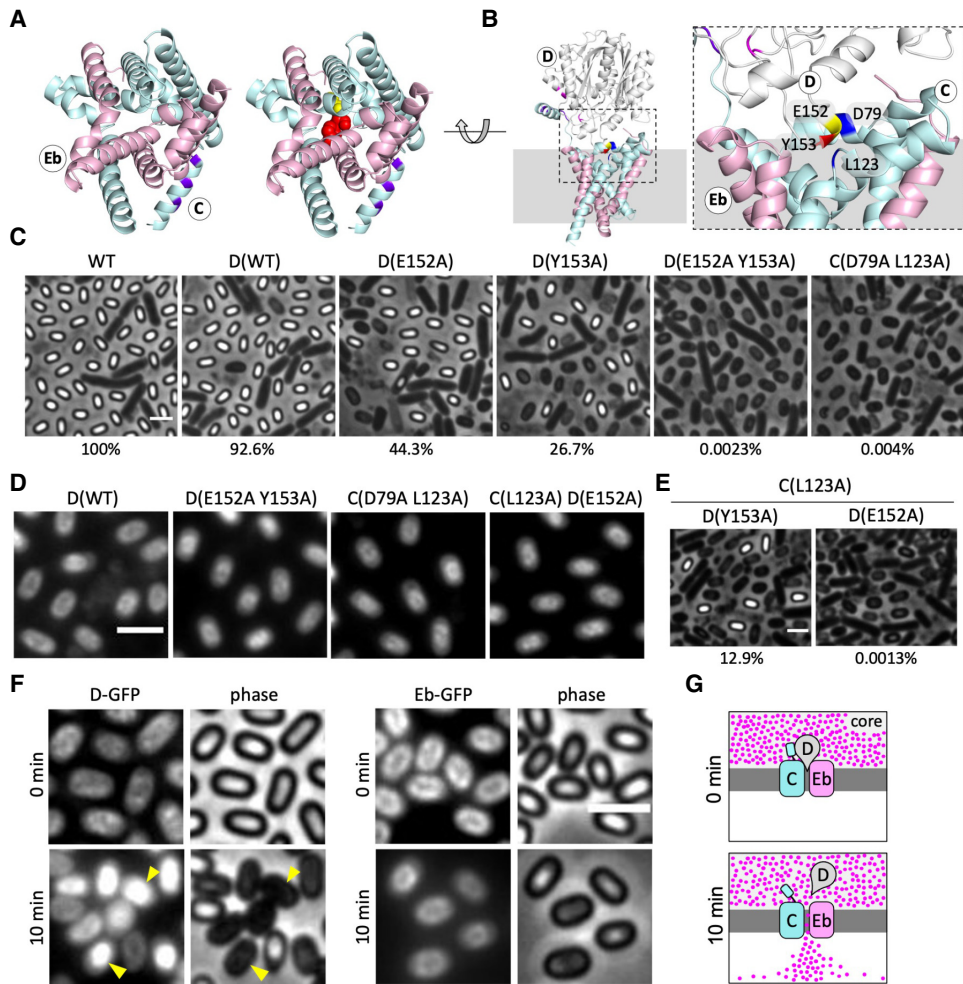


Figure 6. The D protein has plug-like properties. **(A)** AlphaFold model of the C-Eb membrane complex viewed from the integument layers. E152 (yellow) and Y153 (red) in the flexible loop of D appear to plug the channel. The N terminus of C that interacts with D is highlighted in purple as in Figure 4A. **(B)** AlphaFold model of the C-D-Eb complex with E152 (yellow) and Y153 (red) in D and D79 and L123 (blue) in C highlighted. **(C)** Representative phase-contrast images and sporulation efficiencies of the indicated strains. **(D)** Representative fluorescent images of D-GFP localization in spores of the indicated strains. All strains in D harbor *ΔsleB* to maintain the protective cortex layer. **(E)** Representative phase-contrast images and sporulation efficiencies of the indicated double mutants. The complete set of single and double mutants is shown in [Supplemental Figure S17](#). **(F)** Representative phase-contrast and fluorescent images of D-GFP and Eb-GFP localization in purified spores before and 10 min after exposure to 1 mM L-alanine. Examples of germinated phase-dark spores with cytoplasmic D-GFP are indicated (yellow arrowheads). **(G)** Schematic model of the plugged and unplugged C-Eb membrane channel during germination. Scale bars, 2 μ m.

localized to the spore membrane in a manner that resembled wild type (Fig. 6D). These results suggest that D (E152A Y153A) can dock onto the putative C-Eb membrane channel but is impaired in DPA transport and/or in preventing it from leaking out.

In a complementary set of experiments, we generated an alanine substitution at residue D79 in C that evolutionarily covaries with D(E152) and is in close proximity in the predicted structure (Fig. 6B). We also constructed an alanine substitution at L123 in C that is adjacent to D(Y153) in the AlphaFold model (Fig. 6B). The C(D79A) and C(L123A) mutants had modest defects in sporulation that correlated with an increase in premature germination (Supplemental Fig. S17). The double mutant had a synergistic defect in sporulation and a concomitant increase

in premature germination (Fig. 6C; [Supplemental Fig. S17](#)). Importantly, D-GFP displayed a membrane localization pattern that resembled wild type (Fig. 6D). Finally, we combined individual point mutations in D with C(D79A) and, separately, C(L123A). Consistent with the AlphaFold prediction and the evolutionary covariation analysis, combining mutations in residues predicted to interact did not dramatically enhance the phenotypes of the individual mutants (Fig. 6E; [Supplemental Fig. S17](#)). However, we observed synergistic defects when we combined mutations predicted to disrupt the two interactions (Fig. 6E; [Supplemental Fig. S17](#)). In all cases, D-GFP membrane localization was unaffected. Collectively, these results validate the predicted structure and are consistent with a model in which E152 and Y153 in the unstructured loop

Gao et al.

of D insert into the C–Eb membrane channel and facilitate DPA transport and/or prevent DPA from leaking out during spore development.

As with the mutants that impaired the docking of D onto the membrane complex, deletion of *gerA* suppressed the reduction in sporulation efficiency of the D and C mutants that were predicted to disrupt the plug, consistent with a role for this region in DPA import (Supplemental Figs. S17, S18A). All the mutants that disrupted one of the two interactions in the putative plug sporulated at wild-type levels in the Δ *gerA* background. The double mutants that targeted both interactions were suppressed ~50-fold to 0.15%–0.86% sporulation efficiency (Supplemental Figs. S17, S18A). However, the percentages of phase-bright spores in the sporulated cultures were significantly higher (30%–50%) (Supplemental Fig. S18). To investigate this discrepancy, we purified the phase-bright spores using a Histodenz step gradient and analyzed their DPA content. The purified spores from these double mutants appeared less phase-bright than wild type (Supplemental Fig. S18A) and had threefold to fourfold less DPA (Supplemental Fig. S18B). Importantly, the double mutant spores were unable to retain their DPA when incubated for 30 min at 70°C (Supplemental Fig. S18B), explaining the low sporulation efficiency of these mutants. This heat treatment is routinely used to activate spores prior to germination and had no impact on wild type, the mutants that disrupted a single interaction in the plug, or mutants impaired in docking D (Supplemental Fig. S18B). The double-mutant spores also leaked ~50% their DPA over the course of 4 d at 37°C (Supplemental Fig. S19). Finally, spore germination assays revealed that the Δ *gerA*-suppressed double mutants were able to respond to the mixture of asparagine, glucose, fructose, and K⁺ (AGFK) without heat activation (Supplemental Fig. S18C). In contrast, wild-type spores failed to respond to these germinants without prior incubation for 30 min at 70°C (Supplemental Figs. S12, S18C). Collectively, these data indicate that the interaction between D and the cytoplasmic entrance to the predicted C–Eb channel is critical for DPA accumulation during sporulation, DPA retention in the spore core during dormancy, and export during germination, strongly supporting the model that D functions as a cytoplasmic plug.

To investigate whether DPA release during germination involves unplugging the putative C–Eb channel, we visualized D-GFP by fluorescence microscopy during a germination time course. As shown above and in Figure 6D, D-GFP was membrane-associated in dormant spores. However, within 10 min of exposure to L-alanine, D-GFP localized to the cytoplasm in the spores that had transitioned from phase-bright to phase-dark (Fig. 6F). By 20 min, the majority of spores had cytoplasmic D-GFP and were phase-dark (Supplemental Fig. S20). In contrast, Eb-GFP remained membrane-localized throughout the germination time course (Fig. 6F; Supplemental Fig. S20). Collectively, these data suggest that D functions to retain DPA in the spore core during dormancy and that its unplugging during germination enables its release (Fig. 6G) and the activation of cortex lytic enzymes.

Discussion

Collectively, our data argue that C, D, and Eb form a minimal DPA transport complex that functions to import DPA into the developing spore during sporulation and reciprocally releases it in response to nutrient detection during germination. The AlphaFold model and our *in vivo* analysis further suggest that C and Eb form a membrane channel and that D functions as a cytoplasmic plug. The mechanism of transport and the source of energy required to translocate DPA up the steep concentration gradient during sporulation remain unclear. However, our data are consistent with a model in which transport involves continuous rounds of unplugging and replugging of the channel as DPA accumulates in the core, with the plug serving to prevent the occurrence of a fully open channel conformation that would allow DPA to flow down its concentration gradient. In this way, the plug would allow the transporter to achieve an alternating access mechanism of membrane transport (Drew and Boudker 2016). In the context of this model, we hypothesize that the tight coupling between inward and outward open states is partially compromised in the C and D plug mutants, permitting occasional backflow that results in slower DPA import and reduced total accumulation. In regard to germination, our analysis suggests that in response to nutrient sensing, the removal of D opens the channel, enabling DPA release down its concentration gradient. Our data indicate that there are at least two points of contact between D and the C–Eb membrane complex: (1) The cytoplasmic N terminus of C interacts with D and docks it onto the C–Eb membrane complex, and (2) the D loop interacts with the cytoplasmic opening of the predicted C–Eb channel. Impairing either of these interactions sensitizes spores to DPA release in response to nutrients. We hypothesize that nutrient detection by the GerA complex (Artzi et al. 2021) triggers disruption of the interaction between D and the N terminus of C, which in turn causes unplugging of the C–Eb channel and DPA release. Finally, our data suggest that B acts as a regulator or cofactor of the transport complex and A acts as a potential interaction partner of B. However, the role of these factors, as well as Ea and F, in DPA uptake and/or release remains to be elucidated.

We note that *C. difficile* encodes only the core components C, D, and Eb, which were recently proposed to form a membrane complex required for DPA uptake (Donnelly et al. 2016; Francis and Sorg 2016; Baloh and Sorg 2021). Based on the structural predictions using AlphaFold and our evolutionary covariation analysis, we hypothesize that these three proteins function similarly, with D serving as a cytoplasmic plug of the C–Eb channel. Interestingly, studies on germination in *C. difficile* suggest that changes in membrane tension are required for DPA release (Francis and Sorg 2016). Specifically, it was found that germination in the presence of high osmolyte concentrations impaired the release of DPA. Our data suggest that the regulated step in DPA release is the disruption of the interaction between the N terminus of C and D, which leads to unplugging of the membrane channel. It is possible that this interaction could be regulated by

changes in membrane tension. However, it is also possible that once unplugged, channel opening additionally requires a change in membrane tension. Tight control of DPA release, in which two requirements must be satisfied, would not be unreasonable given the irreversibility of this key step in germination. The underlying mechanisms by which nutrient detection triggers DPA release by the C–D–Eb transporter complex represent a major unanswered question for future investigation.

One additional finding that emerged from this study is that sporulating cells that are impaired in DPA accumulation, like the C and D point mutants, have two distinct outcomes: Either they accumulate levels of DPA similar to wild type and form phase-bright, stress-resistant spores, or they undergo premature germination, producing phase-dark and lysed spores. Importantly, the $\Delta gerA$ mutant largely suppressed the premature germination in these mutants, resulting in a larger population of phase-bright spores with wild-type levels of DPA. We therefore hypothesize that a critical window of time exists for DPA to reach a threshold concentration in the spore core to prevent inappropriate activation of GerA and premature germination. If this threshold is not reached because transport is partially impaired, GerA triggers germination. However, if the threshold is reached, germination is not induced, and DPA accumulation can proceed, albeit inefficiently. If correct, this model predicts that many if not all of the mutants previously reported to cause premature germination that are suppressed by $\Delta gerA$ (Ramírez-Guadiana et al. 2017b) impact the rate of DPA accumulation in the developing spore. We suspect that most of these factors indirectly affect DPA import, while a small subset could function as regulators or cofactors of the C–D–Eb complex. The characterization of these factors and the molecular basis of GerA activation when this threshold level of DPA is not achieved remain interesting areas of investigation for the future.

Materials and methods

General methods

All strains in this study were derived from *Bacillus subtilis* 168 (Zeigler et al. 2008). Sporulation was induced by nutrient exhaustion in Difco sporulation medium (DSM) (Schaeffer et al. 1965) for 30 h at 37°C or by resuspension according to the method of Sternlini and Mandelstam (1969). Sporulation efficiency was determined by comparing the heat-resistant (20 min at 80°C) colony-forming units (CFUs) of mutants with wild-type heat-resistant CFUs. All in-frame deletion mutants were derived from *B. subtilis* knockout collection (BKE) (Koo et al. 2017) or generated by transforming isothermal assembled PCR products into *B. subtilis* 168. The antibiotic cassette in the deletion mutants was excised using a temperature-sensitive plasmid that constitutively expresses Cre recombinase (Meeske et al. 2015). All site-directed C and D mutants were generated using QuickChange. All strains, plasmids, and primers used in this study are listed in Supplemental Tables S1, S2, and S3. Plasmid constructions are described in the Supplemental Material. All experiments presented were from one of three biological replicates. All DPA quantification assays, DPA release assays, and germination assays were performed in technical triplicates.

Spore purification with lysozyme and SDS

Total spores were purified from sporulated cells grown in liquid DSM for 30 h at 37°C. Cultures were pelleted and washed three times with ddH₂O. Pellets were resuspended in 1× PBS with 1.5 mg/mL lysozyme and incubated for 1 h at 37°C. SDS was then added to the final concentration of 2% (w/v) and incubated for 30 min at 37°C. Spores were washed five times with ddH₂O and assayed for DPA content, cytologically, or immunoblot analysis.

Spore purification with Histodenz step gradient

Cells were grown in liquid DSM medium at 37°C to an OD₆₀₀ of 0.3 and then spread on DSM agar plates and incubated for 96 h at 37°C. Spores were harvested and washed three times with ddH₂O. The spore pellet was resuspended in 350 μ L of 20% Histodenz (Sigma-Aldrich) and layered on top of 1 mL of 50% Histodenz. The step gradient was subjected to centrifugation at 15,000 rpm for 30 min. The pellet fraction was collected and washed four times with ddH₂O and stored at 4°C. The pellet fraction contained >95% phase-bright spores as assayed by phase-contrast microscopy.

DPA quantification

All purified spores were normalized to an OD₆₀₀ of 1 in 1 mL of ddH₂O, and spore suspensions were incubated for 30 min at 100°C to release DPA. After centrifugation at 15,000 rpm for 5 min, 300 μ L of supernatant was collected and mixed with 300 μ L of 100 μ M TbCl₃. One-hundred-fifty microliters of the mixture was transferred to a black, flat-bottom, 96-well plate, and the fluorescence signal was measured at 545 nm with excitation set at 272 nm using an Infinite M Plex plate reader (Tecan). Each sample was analyzed in technical triplicates and compared with a standard curve to determine the DPA concentration.

DPA release assay

Histodenz step gradient-purified phase-bright spores were normalized to OD₆₀₀ of 1 in 25 mM HEPES (pH 7.4) and were heat-activated for 30 min at 70°C, followed by incubation for 15 min on ice. Seventy-five microliters of spore suspension was transferred to a black, flat-bottom, 96-well plate. An equal volume of 1 mM L-alanine, 10 mM AGFK (10 mM L-asparagine, D-glucose, fructose, and KCl), or buffer (25 mM HEPES at pH 7.4) was added in the 96-well plate. All nutrients and buffer contained 100 μ M TbCl₃, resulting in a final concentration of TbCl₃ of 50 μ M. The fluorescence was monitored at 545 nm with excitation at 272 nm every 2 min for 2 h in an Infinite M Plex plate reader (Tecan). The 96-well plate was maintained at 30°C and agitated between measurements. All spore samples and conditions were tested in technical triplicate and compared with a standard curve to determine DPA release.

DPA leakage assay

Histodenz step gradient-purified phase-bright spores were normalized to an OD₆₀₀ of 1 in 6 mL of 25 mM HEPES (pH 7.4) and incubated at 37°C. Five-hundred microliters of spore suspension was collected at 0, 24, 48, 72, and 96 h. One-hundred microliters of the suspension was serially diluted and assayed for heat-resistant (20 min at 80°C) CFUs. The percentage spore viability was determined by comparing heat-resistant CFUs relative to 0 h. The remaining 400 μ L of spore suspension was pelleted by centrifugation at 15,000 rpm for 5 min, the supernatant was mixed with TbCl₃ (50 μ M final), and DPA was quantified as described

Gao et al.

above. The percentage of DPA in the buffer was determined by comparison with the total DPA released from an equal volume of spores at time 0 h after boiling for 30 min.

Germination assay

Histodenz step gradient-purified phase-bright spores were normalized to an OD₆₀₀ of 1.2 in 25 mM HEPES (pH 7.4) and heat-activated for 30 min at 70°C, followed by incubation for 15 min on ice. One-hundred microliters of spore suspension was transferred to a clear, flat-bottom, 96-well plate, and an equal volume of 1 mM L-alanine, 10 mM AGFK, or the buffer (25 mM HEPES at pH 7.4) was added. The OD₆₀₀ was measured every 2 min for 4 h using an Infinite M Plex plate reader (Tecan). The 96-well plate was maintained at 37°C with agitation between measurements. All spore samples and conditions were tested in technical triplicate.

Microscopy

The sporulation cultures and purified phase-bright spores were concentrated by centrifugation and then immobilized on 2% agarose pads. Phase-contrast and fluorescence microscopy were performed using a Nikon TE2000 inverted microscope equipped with Plan Apo 100×/1.4 oil Ph3 DM objective lens and CoolSNAP HQ2 monochrome CCD camera (Photometrics). The exposure times for phase-contrast, GFP, and mScarlett were 250 msec, 800 msec, and 1 sec, respectively. Image analysis and processing were performed using Fiji or MetaMorph software (Molecular Devices, version 7.7).

Immunoblot analysis

Spores purified with lysozyme and SDS were resuspended in 500 μL of 1× PBS (OD₆₀₀ of spores was ~10) supplemented with 1 mM phenylmethylsulfonyl fluoride (PMSF; Sigma-Aldrich) and transferred to 2-mL tubes containing lysis matrix B (MP Biomedicals). The spores were incubated for 15 min on ice and then lysed using a FastPrep (MP Biomedicals) with 6.5 m/sec for 60 sec. An equal volume of 2× Laemmli sample buffer containing 10% β-mercaptoethanol was immediately added to the lysate. After centrifugation at 15,000 rpm for 5 min, the supernatant was collected, and total protein was determined by noninterfering protein assay (G-Biosciences). Protein concentrations were normalized, and samples were resolved by SDS-PAGE on 17.5% polyacrylamide gels and transferred to an Immobilon-P membrane (Millipore). The membrane was blocked in 5% nonfat milk in 1× PBS with 0.5% Tween-20 (PBST) and probed with anti-His (1:4000; GenScript), anti-GerBC (1:5000) (Stewart et al. 2012), anti-SpoVAD (1:10,000) (Vepechedu and Setlow 2005), anti-GFP (1:5000) (Rudner and Losick 2002), anti-FLAG (1:5000; Sigma-Aldrich F7425), or anti-ProC (1:1000; Invitrogen) diluted in 3% BSA in PBST. The primary antibodies were detected with antimouse (1:20,000) or antirabbit (1:3000) secondary antibodies coupled to horseradish peroxidase (Bio-Rad) and detected by Western Lighting ECL reagent (PerkinElmer).

Structural modeling with AlphaFold 2.0

Protein structures were modeled using AlphaFold 2.0 and ColabFold run locally (see <https://github.com/YoshitakaMo/localcolabfold> for more details; Jumper et al. 2021; Mirdita et al. 2021). The parameters for the run were as follows: The maximum number of model recycling was set to 3. The multiple sequence alignment (MSA) was built using mmseqs2. Sequences from the

same operon were paired in the MSA, and both paired and unpaired sequences were used to generate models. Five models were generated. Models were relaxed using AMBER and ranked by pTM score, and the top-ranked model is shown here; templates were not used.

Evolutionary covariation analysis

Monomer alignments for SpoVAD and SpoVAC were generated using Jackhmmer software (Johnson et al. 2010) with five iterations against the UniRef100 data set (Suzek et al. 2015) downloaded October 2019 across a range of normalized bitscores. A representative alignment was chosen manually for each monomer to carry forward in the analysis, based on maximizing sequence depth versus coverage. The chosen SpoVAD alignment consisted of 4554 sequences with 97.6% coverage, using a column coverage threshold of at least 70% nongap characters with fragments filtered at a threshold of 70%. The SpoVAC alignment consisted of 3923 sequences with 93.3% coverage under the same column coverage and fragment thresholds. The two alignments were then concatenated using the EVcouplings complex pipeline with the “best hits” protocol (available at <https://github.com/debbiemarkslab/EVcouplings>, version 0.0.5; Hopf et al. 2019). The resulting concatenated alignment, with the column coverage threshold changed to 50% and the θ parameter set to 0.9, contained 2011 sequences and had 96.7% of residue positions across both protein sequences meet our coverage threshold. This software was then used to infer parameters used to calculate evolutionary coupling scores for all possible pairs of residues, both for intramonomer and intermonomer possible contacts.

Copurification of *B. cereus* SpoVAC-1, SpoVAD-1, and SpoVAE-1

The plasmids pYG241 (kan) and pYG82 (amp) or pYG239 (amp) were cotransformed into *E. coli* BL21(DE3) containing pAM174 (Meeske et al. 2016), and the resulting expression strains were grown in 1 L of Terrific broth supplemented with 0.4% glycerol, 0.1% glucose, 2 mM MgCl₂, 100 μg/mL ampicillin, 25 μg/mL kanamycin, and 20 μg/mL chloramphenicol at 37°C with shaking until OD₆₀₀ of 0.2. The cultures were then transferred to a 20°C shaking incubator. When the OD₆₀₀ reached 0.7, IPTG (0.5 mM final) and arabinose (0.1% final) were added. Eighteen hours after induction, cells were harvested by centrifugation at 8000g for 15 min at 4°C. The cell pellet was resuspended in 45 mL of lysis buffer (50 mM HEPES at pH 7.6, 150 mM NaCl, 20 mM MgCl₂, 0.5 mM DTT) with 5 U/L benzonase (Sigma E1014), and lysed by two passages through a cell disruptor (Constant System) at 25,000 psi. The lysate was subjected to ultracentrifugation at 35,000 rpm for 1 h at 4°C. The membrane pellet was homogenized in solubilization buffer (20 mM HEPES at pH 7.6, 150 mM NaCl, 20% glycerol, 1% n-dodecyl-β-D-maltopyranoside [DDM; Thermo Fisher]) and rotated for 1 h at 4°C. The mixture was subjected to ultracentrifugation at 35,000 rpm for 1 h at 4°C and the supernatant was collected and supplemented with 2 mM CaCl₂. The DDM-solubilized proteins were loaded on M1 α-Flag antibody resin. The resin was washed with 25 column volumes (CVs) of wash buffer (20 mM HEPES at pH 7.6, 150 mM NaCl, 20% glycerol, 2 mM CaCl₂, 0.1% DDM), and the bound proteins were eluted from the column with five CVs of elution buffer (20 mM HEPES at pH 7.6, 150 mM NaCl, 10% glycerol, 0.1% DDM, 5 mM EDTA at pH 8.0, 0.2 mg/mL FLAG peptide). The eluted proteins were resolved by SDS-PAGE on a 17.5% polyacrylamide gel and visualized by InstantBlue Coomassie staining (ISB1L) or immunoblot as described above. Individual Coomassie-stained bands were excised and treated with chymotrypsin, and

the eluted peptides were identified by mass spectrometry (MS; Taplin Mass Spectrometry Facility, Harvard Medical School). The MS identified 12 unique peptides for the C subunit, 25 unique peptides for the D subunit, and one unique peptide for the Eb subunit. We note that the pYG241 contains T7 promoters fused to both spoVAD1-His and His-spoVAB1; however, His-SpoVAB1 was undetectable in the induced culture based on anti-His immunoblot and was not characterized further.

Competing interest statement

The authors declare no competing interests.

Acknowledgments

We thank all members of the Bernhardt-Rudner supergroup past and present for helpful advice, discussions, and encouragement; Lior Artzi for feedback and discussion; Paula Montero Llopis and the Harvard Medical School Microscopy Resources on the North Quad (MicRoN) Core for advice on microscopy; and the Research Computing Group at the Harvard Medical School for structural modeling using the O2 High-Performance Computing Cluster. We thank Reviewer #3 for alerting us to the discrepancy between the sporulation efficiency and percentage of phase-bright spores in the plug mutants. Finally, we acknowledge Peter Setlow for antibodies and inspiration. Support for this work comes from GM086466, GM127399, and DARPA HR001117S0029 to D.Z.R., and funds from the Harvard Medical School Dean's Initiative to D.S.M., A.C.K., and D.Z.R. J.D.A. was funded by National Institutes of Health grant F32GM130003.

Author contributions: Y.G. conceived and designed the study; acquired, analyzed, and interpreted the data; wrote the draft of the manuscript and gave final approval; and is accountable for the data. R.D.C.B.-O. designed the study, acquired the data, and edited the manuscript. J.D.A. designed the study, acquired and analyzed the data, and edited the manuscript. F.H.R.-G. designed the study, acquired the data, and edited the manuscript. A.A. acquired the data and edited the manuscript. K.P.B. acquired and analyzed the data and edited the manuscript. D.S.M. conceived and designed the study and gave final approval. A.C.K. conceived and designed the study, analyzed and interpreted the data, edited the manuscript, and gave final approval. D.Z.R. conceived and designed the study, analyzed and interpreted the data, wrote the draft of the manuscript, gave final approval, and is accountable for the data.

References

- Amon JD, Artzi L, Rudner DZ. 2021. Genetic evidence for signal transduction within the *Bacillus subtilis* GerA germinant receptor. *J Bacteriol* **204**: e0047021. doi:10.1128/JB.00470-21
- Artzi L, Alon A, Brock KP, Green AG, Tam A, Ramírez-Guadiana FH, Marks D, Kruse A, Rudner DZ. 2021. Dormant spores sense amino acids through the B subunits of their germination receptors. *Nat Commun* **12**: 6842. doi:10.1038/s41467-021-27235-2
- Bach ML, Gilvarg C. 1966. Biosynthesis of dipicolinic acid in sporulating *Bacillus megaterium*. *J Biol Chem* **241**: 4563–4564. doi:10.1016/S0021-9258(18)99755-3
- Baloh M, Sorg JA. 2021. *Clostridioides difficile* SpoVAD and SpoVAE interact and are required for dipicolinic acid uptake into spores. *J Bacteriol* **203**: e0039421. doi:10.1128/JB.00394-21
- Berendsen EM, Boekhorst J, Kuipers OP, Wells-Bennik MH. 2016a. A mobile genetic element profoundly increases heat resistance of bacterial spores. *ISME J* **10**: 2633–2642. doi:10.1038/ismej.2016.59
- Berendsen EM, Koning RA, Boekhorst J, de Jong A, Kuipers OP, Wells-Bennik MH. 2016b. High-level heat resistance of spores of *Bacillus amyloliquefaciens* and *Bacillus licheniformis* results from the presence of a spoVA operon in a Tn1546 transposon. *Front Microbiol* **7**: 1912. doi:10.3389/fmicb.2016.01912
- Daniel RA, Errington J. 1993. Cloning, DNA sequence, functional analysis and transcriptional regulation of the genes encoding dipicolinic acid synthetase required for sporulation in *Bacillus subtilis*. *J Mol Biol* **232**: 468–483. doi:10.1006/jmbi.1993.1403
- Donnelly ML, Fimlaid KA, Shen A. 2016. Characterization of *Clostridium difficile* spores lacking either SpoVAC or dipicolinic acid synthetase. *J Bacteriol* **198**: 1694–1707. doi:10.1128/JB.00986-15
- Drew D, Boudker O. 2016. Shared molecular mechanisms of membrane transporters. *Annu Rev Biochem* **85**: 543–572. doi:10.1146/annurev-biochem-060815-014520
- Fort P, Errington J. 1985. Nucleotide sequence and complementation analysis of a polycistronic sporulation operon, spoVA, in *Bacillus subtilis*. *J Gen Microbiol* **131**: 1091–1105.
- Francis MB, Sorg JA. 2016. Dipicolinic acid release by germinating *Clostridium difficile* spores occurs through a mechano-sensing mechanism. *mSphere* **1**: e00306-16. doi:10.1128/mSphere.00306-16
- Heffron JD, Sherry N, Popham DL. 2011. In vitro studies of peptidoglycan binding and hydrolysis by the *Bacillus anthracis* germination-specific lytic enzyme SleB. *J Bacteriol* **193**: 125–131. doi:10.1128/JB.00869-10
- Hopf TA, Colwell LJ, Sheridan R, Rost B, Sander C, Marks DS. 2012. Three-dimensional structures of membrane proteins from genomic sequencing. *Cell* **149**: 1607–1621. doi:10.1016/j.cell.2012.04.012
- Hopf TA, Green AG, Schubert B, Mersmann S, Schärfe CPI, Ingraham JB, Toth-Petroczy A, Brock K, Riesselman AJ, Palmedo P, et al. 2019. The EVcouplings Python framework for coevolutionary sequence analysis. *Bioinformatics* **35**: 1582–1584. doi:10.1093/bioinformatics/bty862
- Johnson LS, Eddy SR, Portugaly E. 2010. Hidden Markov model speed heuristic and iterative HMM search procedure. *BMC Bioinformatics* **11**: 431. doi:10.1186/1471-2105-11-431
- Jumper J, Evans R, Pritzel A, Green T, Figurnov M, Ronneberger O, Tunyasuvunakool K, Bates R, Žídek A, Potapenko A, et al. 2021. Highly accurate protein structure prediction with AlphaFold. *Nature* **596**: 583–589. doi:10.1038/s41586-021-03819-2
- Kall L, Krogh A, Sonnhammer EL. 2007. Advantages of combined transmembrane topology and signal peptide prediction—the Phobius web server. *Nucleic Acids Res* **35**: W429–W432. doi:10.1093/nar/gkm256
- Koo BM, Kritikos G, Farelli JD, Todor H, Tong K, Kimsey H, Wapinski I, Galardini M, Cabal A, Peters JM, et al. 2017. Construction and analysis of two genome-scale deletion libraries for *Bacillus subtilis*. *Cell Syst* **4**: 291–305.e7. doi:10.1016/j.cels.2016.12.013
- Korza G, Setlow P. 2013. Topology and accessibility of germination proteins in the *Bacillus subtilis* spore inner membrane. *J Bacteriol* **195**: 1484–1491. doi:10.1128/JB.02262-12
- Krogh A, Larsson B, von Heijne G, Sonnhammer EL. 2001. Predicting transmembrane protein topology with a hidden Markov model: application to complete genomes. *J Mol Biol* **305**: 567–580. doi:10.1006/jmbi.2000.4315

Gao et al.

- Li Y, Davis A, Korza G, Zhang P, Li YQ, Setlow B, Setlow P, Hao B. 2012. Role of a SpoVA protein in dipicolinic acid uptake into developing spores of *Bacillus subtilis*. *J Bacteriol* **194**: 1875–1884. doi:10.1128/JB.00062-12
- Marks DS, Colwell LJ, Sheridan R, Hopf TA, Pagnani A, Zecchina R, Sander C. 2011. Protein 3D structure computed from evolutionary sequence variation. *PLoS One* **6**: e28766. doi:10.1371/journal.pone.0028766
- Meeske AJ, Sham LT, Kimsey H, Koo BM, Gross CA, Bernhardt TG, Rudner DZ. 2015. Murj and a novel lipid II flippase are required for cell wall biogenesis in *Bacillus subtilis*. *Proc Natl Acad Sci* **112**: 6437–6442. doi:10.1073/pnas.1504967112
- Meeske AJ, Riley EP, Robins WP, Uehara T, Mekalanos JJ, Kahne D, Walker S, Kruse AC, Bernhardt TG, Rudner DZ. 2016. SEDS proteins are a widespread family of bacterial cell wall polymerases. *Nature* **537**: 634–638. doi:10.1038/nature19331
- Mirdita M, Ovchinnikov S, Steinegger M. 2021. ColabFold—making protein folding accessible to all. *bioRxiv* doi:10.1101/2021.08.15.456425
- Moir A, Cooper G. 2015. Spore germination. *Microbiol Spectr* doi:10.1128/microbiolspec.TBS-0014-2012
- Moriyama R, Hattori A, Miyata S, Kudoh S, Makino S. 1996. A gene (*sleB*) encoding a spore cortex-lytic enzyme from *Bacillus subtilis* and response of the enzyme to L-alanine-mediated germination. *J Bacteriol* **178**: 6059–6063. doi:10.1128/jb.178.20.6059-6063.1996
- Paredes-Sabja D, Setlow P, Sarker MR. 2011. Germination of spores of *Bacillales* and *Clostridiales* species: mechanisms and proteins involved. *Trends Microbiol* **19**: 85–94. doi:10.1016/j.tim.2010.10.004
- Perez-Valdespino A, Li Y, Setlow B, Ghosh S, Pan D, Korza G, Feeherry FE, Doona CJ, Li YQ, Hao B, et al. 2014. Function of the SpoVAEa and SpoVAF proteins of *Bacillus subtilis* spores. *J Bacteriol* **196**: 2077–2088. doi:10.1128/JB.01546-14
- Popham DL, Illades-Aguilar B, Setlow P. 1995. The *Bacillus subtilis* dacB gene, encoding penicillin-binding protein 5*, is part of a three-gene operon required for proper spore cortex synthesis and spore core dehydration. *J Bacteriol* **177**: 4721–4729. doi:10.1128/jb.177.16.4721-4729.1995
- Powell JF. 1953. Isolation of dipicolinic acid (pyridine-2:6-dicarboxylic acid) from spores of *Bacillus megatherium*. *Biochem J* **54**: 210–211. doi:10.1042/bj0540210
- Ramírez-Guadiana FH, Meeske AJ, Rodrigues CDA, Barajas-Ornelas RDC, Kruse AC, Rudner DZ. 2017a. A two-step transport pathway allows the mother cell to nurture the developing spore in *Bacillus subtilis*. *PLoS Genet* **13**: e1007015. doi:10.1371/journal.pgen.1007015
- Ramírez-Guadiana FH, Meeske AJ, Wang X, Rodrigues CDA, Rudner DZ. 2017b. The *Bacillus subtilis* germinant receptor GerA triggers premature germination in response to morphological defects during sporulation. *Mol Microbiol* **105**: 689–704. doi:10.1111/mmi.13728
- Rudner DZ, Losick R. 2002. A sporulation membrane protein tethers the pro- α K processing enzyme to its inhibitor and dic-
ates its subcellular localization. *Genes Dev* **16**: 1007–1018. doi:10.1101/gad.977702
- Schaeffer P, Millet J, Aubert JP. 1965. Catabolic repression of bacterial sporulation. *Proc Natl Acad Sci* **54**: 704–711. doi:10.1073/pnas.54.3.704
- Setlow P. 2014. Spore resistance properties. *Microbiol Spectr* doi:10.1128/microbiolspec.TBS-0003-2012
- Setlow P, Wang S, Li YQ. 2017. Germination of spores of the orders *Bacillales* and *Vlostridiales*. *Annu Rev Microbiol* **71**: 459–477. doi:10.1146/annurev-micro-090816-093558
- Shen A, Edwards AN, Sarker MR, Paredes-Sabja D. 2019. Sporulation and germination in clostridial pathogens. *Microbiol Spectr* doi:10.1128/microbiolspec.GPP3-0017-2018
- Sonhammer EL, von Heijne G, Krogh A. 1998. A hidden Markov model for predicting transmembrane helices in protein sequences. *Pro Int Conf Intell Syst Mol Biol* **6**: 175–182.
- Sterlini JM, Mandelstam J. 1969. Commitment to sporulation in *Bacillus subtilis* and its relationship to development of actinomycin resistance. *Biochem J* **113**: 29–37. doi:10.1042/bj1130029
- Stewart KA, Yi X, Ghosh S, Setlow P. 2012. Germination protein levels and rates of germination of spores of *Bacillus subtilis* with overexpressed or deleted genes encoding germination proteins. *J Bacteriol* **194**: 3156–3164. doi:10.1128/JB.00405-12
- Suzek BE, Wang Y, Huang H, McGarvey PB, Wu CH, the UniProt Consortium. 2015. Uniref clusters: a comprehensive and scalable alternative for improving sequence similarity searches. *Bioinformatics* **31**: 926–932. doi:10.1093/bioinformatics/btu739
- Tovar-Rojo F, Chander M, Setlow B, Setlow P. 2002. The products of the *spoVA* operon are involved in dipicolinic acid uptake into developing spores of *Bacillus subtilis*. *J Bacteriol* **184**: 584–587. doi:10.1128/JB.184.2.584-587.2002
- Velásquez J, Schuurman-Wolters G, Birkner JP, Abree T, Poolman B. 2014. *Bacillus subtilis* spore protein SpoVAC functions as a mechanosensitive channel. *Mol Microbiol* **92**: 813–823. doi:10.1111/mmi.12591
- Vepachedu VR, Setlow P. 2004. Analysis of the germination of spores of *Bacillus subtilis* with temperature sensitive *spo* mutations in the *spoVA* operon. *FEMS Microbiol Lett* **239**: 71–77. doi:10.1016/j.femsle.2004.08.022
- Vepachedu VR, Setlow P. 2005. Localization of SpoVAD to the inner membrane of spores of *Bacillus subtilis*. *J Bacteriol* **187**: 5677–5682. doi:10.1128/JB.187.16.5677-5682.2005
- Wang ST, Setlow B, Conlon EM, Lyon JL, Imamura D, Sato T, Setlow P, Losick R, Eichenberger P. 2006. The forespore line of gene expression in *Bacillus subtilis*. *J Mol Biol* **358**: 16–37. doi:10.1016/j.jmb.2006.01.059
- Zeigler DR, Prágai Z, Rodriguez S, Chevreux B, Muffler A, Albert T, Bai R, Wyss M, Perkins JB. 2008. The origins of 168, W23, and other *Bacillus subtilis* legacy strains. *J Bacteriol* **190**: 6983–6995. doi:10.1128/JB.00722-08



The SpoVA membrane complex is required for dipicolinic acid import during sporulation and export during germination

Yongqiang Gao, Rocio Del Carmen Barajas-Ornelas, Jeremy D. Amon, et al.

Genes Dev. 2022, **36**: originally published online June 2, 2022
Access the most recent version at doi:[10.1101/gad.349488.122](https://doi.org/10.1101/gad.349488.122)

Supplemental Material <http://genesdev.cshlp.org/content/suppl/2022/06/01/gad.349488.122.DC1>

References This article cites 48 articles, 19 of which can be accessed free at:
<http://genesdev.cshlp.org/content/36/9-10/634.full.html#ref-list-1>

Creative Commons License This article is distributed exclusively by Cold Spring Harbor Laboratory Press for the first six months after the full-issue publication date (see <http://genesdev.cshlp.org/site/misc/terms.xhtml>). After six months, it is available under a Creative Commons License (Attribution-NonCommercial 4.0 International), as described at <http://creativecommons.org/licenses/by-nc/4.0/>.

Email Alerting Service Receive free email alerts when new articles cite this article - sign up in the box at the top right corner of the article or [click here](#).

